Accelerated Publications

Crystal Structure of the Broadly Cross-Reactive HIV-1-Neutralizing Fab X5 and Fine Mapping of Its Epitope[†,‡]

Ramalakshmi Darbha,[§] Sanjay Phogat,[‖] Aran F. Labrijn,[⊥] Yuuei Shu,[‖] Yijun Gu,[§] Michelle Andrykovitch,[§] Mei-Yun Zhang,[‖] Ralph Pantophlet,[⊥] Loic Martin,[#] Claudio Vita,[#] Dennis R. Burton,[⊥] Dimiter S. Dimitrov,*[,‖] and Xinhua Ji*[,§]

Macromolecular Crystallography Laboratory and Laboratory of Experimental and Computational Biology, National Cancer Institute, Frederick, Maryland 21702, Departments of Immunology and Molecular Biology, The Scripps Research Institute, La Jolla, California 92037, and Protein Engineering and Research Department, CEA Saclay, 91191 GIF-sur-Yvette, France

Received July 24, 2003; Revised Manuscript Received December 27, 2003

ABSTRACT: The human monoclonal antibody Fab X5 neutralizes a broad range of HIV-1 primary isolates. The crystal structure of X5 has been determined at 1.9 Å resolution. There are two crystallographically independent Fab fragments in the asymmetric unit. The crystallographic R value for the final model is 0.22. The antibody-combining site features a long (22 amino acid residues) CDR H3 with a protruding hook-shaped motif. The X5 structure and site-directed mutagenesis data suggest that X5 amino acid residues W100 and Y100F in the CDR H3 motif may be critical for the binding of Fab X5 to gp120. X5 bound to a complex of a CD4 mimetic and gp120 with approximately the same kinetics and affinity as to a CD4−gp120 complex, suggesting that specific interactions between CD4 and X5 are unlikely to contribute to the binding of X5 to gp120−CD4 complexes. Binding of X5 to alanine scanning mutants of gp120JR-CSF complexed with CD4 suggested a critical role of the highly conserved amino acid residues at positions 423 and 432. The X5 structure and fine mapping of its epitope may assist in the elucidation of the mechanisms of viral entry and neutralization, and the development of HIV-1 inhibitors and vaccines.

HIV-1 entry into the host cells is initiated by the interaction of its envelope protein gp120 and host cell receptors CD4 and CCR5 followed by the conformational changes of gp120, ultimately leading to the fusion of the virus and the host cells (*1*, *2*). Characterization of the gp120 structures that are exposed during virus entry and conserved among various isolates may help in the mechanistic studies of HIV-1 fusion and the development of antiviral inhibitors and vaccines. We hypothesized that purified gp120 isolates in complex with receptor molecules exhibit such conserved structures (*1*, *3*) that could be used to select antibodies by screening phage display libraries (*4*); the selected antibodies could then help in the identification and characterization of the conserved structures among gp120 isolates. Using the gp120−CD4−CCR5 complexes as a screening antigen, we recently identified a broadly cross-reactive HIV-1-neutralizing human monoclonal antibody (hMAb) Fab, X5, and found that Fab X5 bound much better to the gp120−CD4 complexes than to the gp120 isolates alone, indicating that it is a CD4-induced (CD4i) Fab (*4*). CD4i Fabs neutralize some T cell-adapted HIV-1 isolates but generally do not exhibit significant neutralizing activity against primary isolates (*5*). Fab X5, however, inhibited gp120-mediated cell fusion of more than 30 primary isolates as potently as the broadly cross-reactive HIV-1-neutralizing hMAb IgG1 b12 [PDB entry 1HZH (*6*, *7*)]. For IgG1 b12 and other non-CD4i HIV-1-neutralizing hMAbs, the IgG1 is more potent than the Fab fragment. For X5, however, the IgG1 is less potent than the Fab and the Fab is less potent than the single-chain Fv (scFv) due, at least in part, to steric factors that limit the access of the antibody to the gp120 epitopes (*8*). Here, we present the crystal structure of Fab X5 with a fine mapping of its epitope based on available structural information and mutagenesis studies. The X5 structure and the fine mapping of its epitope may assist

Table 1: Data Collection and Structure Refinement Statistics for X5

	overall	last shell
data statistics		
resolution range (Å)	30.0−1.9	1.97−1.9
completeness (%)	100.0	99.9
$I/\sigma(I)$	39.7	3.2
R_{scaling}[a]	0.066	0.498
refinement statistics		
resolution range (Å)	30.0−1.9	2.02−1.9
no. of reflections used for refinement with $0\sigma(I)$ cutoff	93615	14575
no. of reflections used for R_{free} calculations	4699	767
crystallographic R[b]	0.22	0.27
R_{free}	0.23	0.29
no. of amino acid residues/average B factor (Å^2)	895/32.8	
no. of water oxygens/average B factor (Å^2)	619/36.1	
rms deviations from ideal geometry		
bond distances (Å)	0.01	
bond angles (deg)	1.46	
Ramachandran plot		
most favored φ and ψ angles (%)	87.4	
disallowed φ and ψ angles (%)	0.4	

[a] $R_{\text{scaling}} = \sum|I - \langle I\rangle|/\sum I$. [b] Crystallographic $R = \sum_{hkl}||F_{\text{o}}| - |F_{\text{c}}||/\sum_{hkl}|F_{\text{o}}|$.

in the mechanistic studies of viral entry and neutralization, and the development of HIV-1 inhibitors and vaccines.

EXPERIMENTAL PROCEDURES

Protein Expression and Purification. Fab X5 was produced as previously described (*4*, *9*). Briefly, a 10 mL column of degassed fast flow protein G (Amersham) in PBS (pH 7.4) was packed and used for purification; 50 mL of cell lysate in 1× PBS supplemented with PMSF at a final concentration of 200 μM was loaded onto the protein G column. The lysate was loaded at a flow rate of 3 mL/min and washed with PBS (pH 7.4). Fab X5 was eluted with 0.5 M acetic acid (pH 3.0); the eluate was collected in a tube containing 1 mL of Tris-HCl (pH 9.0). The fractions containing the protein peak were pooled and concentrated with centriprep columns (10 kDa cutoff), and passed through 0.2 μm low protein binding filters (acrodisc syringe filters from Gelman Labs) under sterile conditions. Fab X5 was finally exchanged in 50 mM Tris-HCl buffer (pH 7.4) and concentrated to 10 mg/mL for crystallization experiments.

Crystallization. Crystals of X5 were grown at 18 ± 1 °C using the sitting drop vapor diffusion technique. The well solution contained 30% 1,2-propanediol and 20% PEG-400 in 0.1 M HEPES buffer (pH 7.5). The 10−15 μL drops, containing equal volumes of protein and well solutions, were equilibrated against 500 μL of well solution. The X5 crystals grew in 3−4 days in the morphology of rectangular rods. The crystals were mounted on nylon loops and frozen in liquid nitrogen before X-ray diffraction data collection.

Data Collection and Structure Determination. The crystals of Fab X5 (space group $P42_12$, unit cell dimensions $a = b = 139.6$ Å and $c = 120.3$ Å) diffracted to 1.9 Å resolution. X-ray diffraction data were collected at beamline X9B of the National Synchrotron Light Source. A cryogenic temperature (100 K) was maintained with an Oxford Cryosystem for the entire data collection. The data were recorded with an ADSC Quantum-4 CCD detector and processed using DENZO and SCALEPACK (*10*). Further data processing was done with SCALEPACK2MTZ, TRUNCATE [for molecular replacement using AMoRe (*11*)], and

MTZ2VARIOUS [for structure refinement using CNS (*12*)], which are embedded in the CCP4 suite (*13*). X-ray data statistics are summarized in Table 1.

We determined the crystal structure of Fab X5 by molecular replacement using AMoRe (*11*) with the constant domains of both light and heavy chains of the mature metal chelatase catalytic antibody from *Homo sapiens* [PDB entry 3FCT (*14*)] as the search model. Two solutions were obtained with a correlation coefficient of 33.7% and a crystallographic R value of 49.8% for X-ray data within the resolution range of 10−4 Å. The model was then subject to rigid body refinement, energy minimization, and grouped B factor refinement before a difference Fourier synthesis was carried out. The difference map revealed the location of two variable domains. The model of the two variable domains was manually built on the basis of similar Fab structures and combined with the two constant domains obtained from molecular replacement, resulting in a complete model containing two Fabs (Mol A and Mol B). On the basis of the difference map as well as the refined electron density, a mutation (H165Q) in the constant domain of the light chain was identified in both Fabs. Model building was carried out with O (*15*) and structure refinement with CNS (*16*). All data within the resolution range of 30.0−1.90 Å were used in the refinement with 5% of the data randomly chosen for R_{free} calculations. Bulk solvent corrections were applied. The final model and statistics are summarized in Table 1. The electron density (omit map) of CDR H3 is shown in Figure 1. The Ramachandran plot showed that three residues fall in the disallowed region, including light chain residue A51 in both Fabs and heavy chain residue D100G in Mol A. The two Ala residues have well-defined electron density and are located in the middle of a γ-turn (A50−A52). The CDR H3 is less than well defined, which could account for the outlier D100G on the Ramachandran plot.

Site-Directed Mutagenesis and Binding Experiments with gp120 and X5. Mutagenesis of gp120$_{\text{JR−SF}}$ and Fab X5 was performed using the QuikChange site-directed mutagenesis kit (Stratagene, La Jolla, CA) according to the manufacturer's protocols. All mutations were confirmed by DNA sequenc-
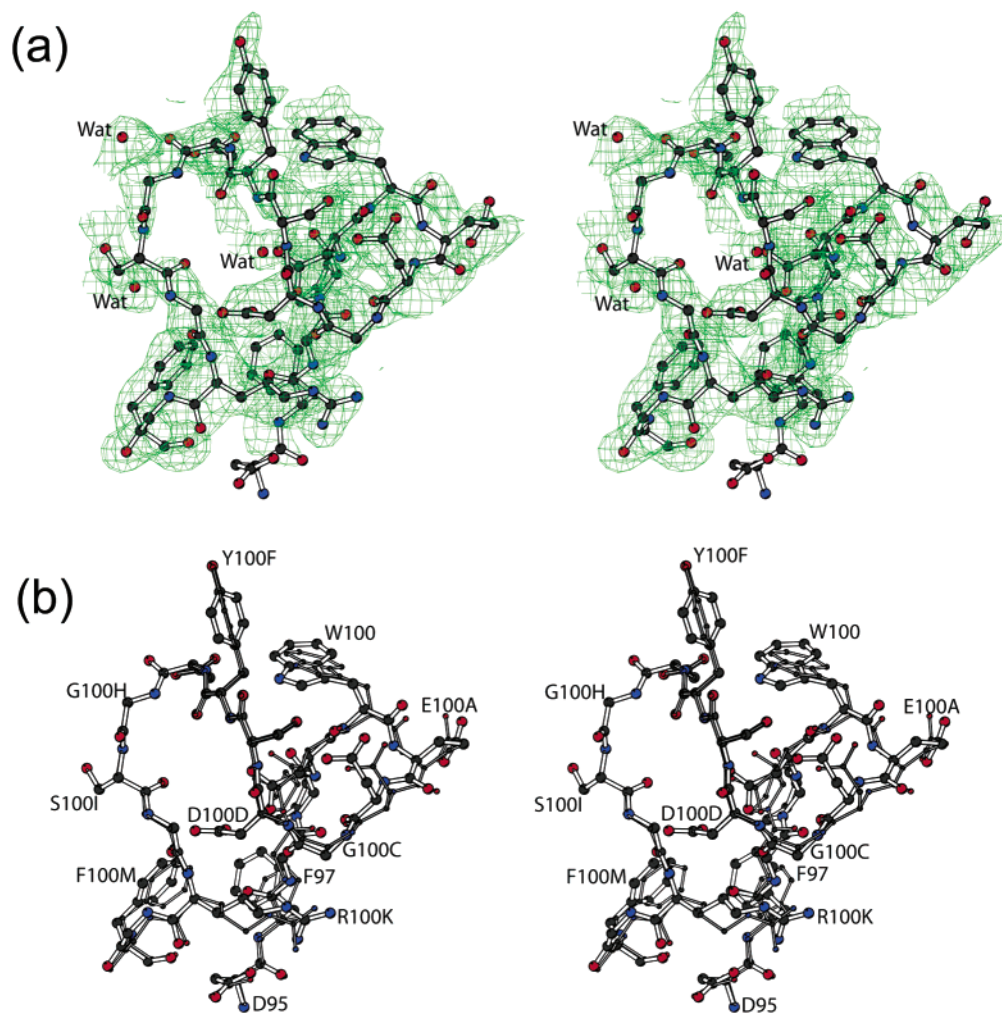
FIGURE 1: Crystal structure of Fab X5. (a) Stereoview showing the hook shape and final $F_o - F_c$ omit map contoured at 2.3σ for the CDR H3 motif of the Fab X5 heavy chain. The protein is illustrated as a ball-and-stick model with the atomic color scheme (carbon in black, nitrogen in blue, and oxygen in red) and the electron density as a green net. (b) Stereoview illustrating the superposition of the two CDR H3 motifs in the two independent X5 molecules, Mol A and Mol B. The thinner model is the CDR H3 motif of Mol B. The rms deviation for all Cα positions between the two CDR H3 motifs is 0.47 Å. The average *B* factors of the CDR H3 motif are 63 and 66 Å² in Mol A and Mol B, respectively; the average *B* factor for all protein atoms is 32 Å². This figure was generated using BOBSCRIPT (*24*).

ing. Studies of binding of the wild-type and mutant Fab X5 to the recombinant gp120 proteins (JR-FL and 89.6) and the gp120−CD4 complexes were performed with 96-well Nunc-Immuno Maxisorp surface plates as previously described (*3*).

BIACORE Surface Plasmon Resonance Analysis. Interaction analyses were performed on a BIA3000 optical biosensor (Biacore AB, Uppsala, Sweden) with simultaneous monitoring of four flow cells. Kinetic studies were performed on a low-charge (B1) sensor chip with Fab X5 immobilized at 250 RU using carbodiimide coupling chemistry. The binding capacity of the surface was kept low to avoid the mass transport effect and steric hindrance. One flow cell was left blank as a control for nonspecific binding and refractive index changes. Flow-independent kinetic parameters showed the absence of mass transport and rebinding effects. The association and dissociation phase data were fitted simultaneously to a 1:1 Langmuir global model by using the nonlinear data analysis program BIAevaluation 3.2. The buffer that was used consisted of 10 mM phosphate, 150 mM NaCl, 3.4 mM EDTA, and 0.005% P-20 (pH 7.4). The following envelope proteins were analyzed: gp120 JRFL (N. Schulke, Progenics, Tarrytown, NY), gp120 $_{W61D}$ (Centralized Facilities for AIDS Reagents, Potters Bar, U.K.), and gp120$_{HXB2}$ (F. Veas,

Montpellier, France). These proteins were premixed with a 5-fold molar excess of CD4 (D1D2, S. Leow, Pharmacia, Kalamazoo, MI) or CD4M33 mini-protein (*17*) at 37 °C for 60 min before injection at a rate of 30 μL/min.

RESULTS AND DISCUSSION

Structure Description. The two Fab X5 molecules (Mol A and Mol B) are structurally similar and pack in an alternate fashion with the constant domains of one Fab interacting with the variable domains of the other. Mol A has a lower *B* factor (27.2 Å²) than Mol B (37.4 Å²). The entire structure is well-defined except for a few N- or C-terminal residues and the two CDR H3 loops. Heavy chain residues 1 and 2 in Mol A and 1−3 in Mol B and C-terminal residues 217−220 in both Fabs have not been located (presumably disordered). The CDR H3 loop of the heavy chain (D95−F102) is less than well defined, as indicated by the poorer electron density starting from P98 to G100J in both Fabs (Figure 1a). The Cα traces of the two CDR H3 loops are very similar, whereas the conformation of their side chains differs (Figure 1b).

Fab 17b has a prominent 19-residue CDR H3 loop (Figure 2a), which dominates the binding of 17b to gp120 (*18*, *19*).
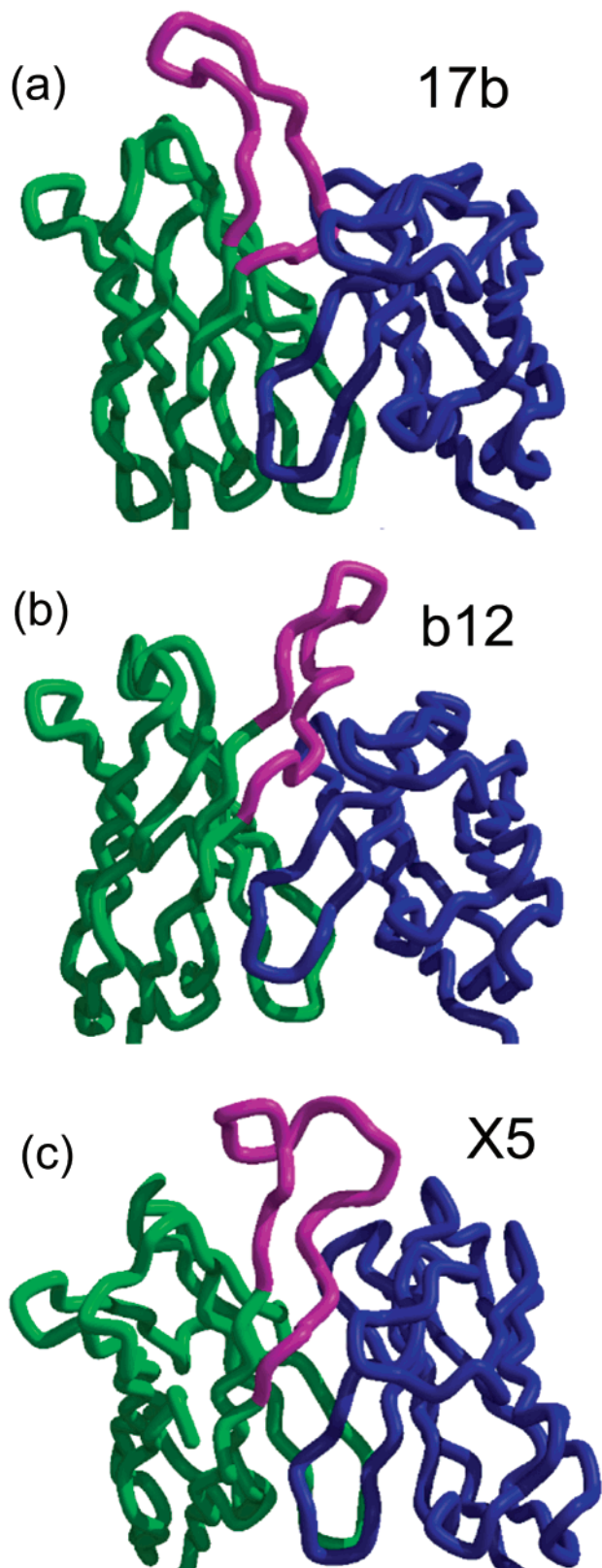
FIGURE 2: Comparison of CDR H3 structures (a) 17b (PDB entry 1G9M), (b) b12 (PDB entry 1HZH), and (c) X5 (this work). The light chain is shown in blue. The heavy chain is in green with the CDR H3 loop in magenta. This figure was generated using BOBSCRIPT (*24*).

Similarly, in IgG1 b12, the 18-residue CDR H3 assumes a finger-like loop (Figure 2b) with a Trp residue at the apex [PDB entry 1HZH (*7*)]. This extended loop likely facilitates the insertion of b12 into the recessed CD4 binding site of gp120. The hook-shaped CDR H3 of Fab X5 (Figure 2c) has two residues (W100 and Y100F) pointing out of the hook (Figure 1a). The hook conformation with the certain flexibility of CDR H3 could be critical for the high affinity of Fab X5 for the CD4 complexes of various HIV-1 isolates.

Possible Interactions between Fab X5 and CD4. To investigate the possibility of direct interactions between Fab X5 and CD4, we measured the affinity of binding of X5 to gp120 in complex with CD4M33, a functional CD4 mimic with 27 amino acid residue and a sequence unrelated to CD4 (*17*), and compared the results with typical affinities of Fab X5 for the gp120−CD4 complex. From binding experiments performed by using an optical biosensor system based on surface plasmon resonance (Figure 3), we determined the following association and dissociation rate constants: $k_{on} = (2.4 \pm 0.02) \times 10^5$ or $(1.3 \pm 0.04) \times 10^5$ M^{-1} s^{-1} and $k_{off} = (0.7 \pm 0.2) \times 10^4$ or $(2.2 \pm 0.1) \times 10^4$ s^{-1} for X5 binding to $gp120_{W61D}$ complexes with sCD4 or CD4M33, respectively; $k_{on} = (2.57 \pm 0.03) \times 10^5$ or $(1.09 \pm 0.03) \times 10^5$ M^{-1} s^{-1} and $k_{off} = (0.5 \pm 0.05) \times 10^4$ or $(0.5 \pm 0.07) \times 10^4$ s^{-1} for ×5 binding to $gp120_{JR-FL}$ complexes with sCD4 or CD4M33, respectively. Similar rate constants were also obtained by using the $gp120_{HXB2}$ envelope (not shown). Equilibrium dissociation constants, obtained from the kinetic parameters, were rather similar. For example, for binding of X5 to $gp120_{W61D}$, K_d equaled $(2.9 \pm 0.9) \times 10^{-10}$ M ($\chi^2 = 3.7$) or $(17 \pm 3) \times 10^{-10}$ M ($\chi^2 = 3.9$) in the presence of sCD4 or CD4M33, respectively. For binding to $gp120_{JRFL}$, K_d equaled $(2.1 \pm 0.2) \times 10^{-10}$ M ($\chi^2 = 5.0$) or $(4.7 \pm 0.7) \times 10^{-10}$ M ($\chi^2 = 2.2$) in the presence of sCD4 or CD4M33, respectively. For binding to $gp120_{HXB2}$, K_d equaled $(5.3 \pm 3) \times 10^{-10}$ M ($\chi^2 = 1.5$) or $(6.2 \pm 0.5) \times 10^{-10}$ M ($\chi^2 = 1.1$) in the presence of sCD4 or CD4M33, respectively. These results indicate that specific interactions between CD4 and X5 are unlikely to contribute to the binding of X5 to the gp120−CD4 complexes.

Site-Directed Mutagenesis of X5 and gp120. On the basis of our crystal structure, X5 residues W100 and Y100F in the CDR H3 motif (Figure 1) may be critical for the binding of Fab X5 to gp120. To test this prediction, we mutated these residues, individually or in combination, to glycine and phenylalanine, respectively. These mutations significantly reduced the affinity of binding of X5 to gp120 isolates JR-FL and 89.6 with and without bound CD4 (Figure 4).

To help localize the X5 epitope, we generated a panel of 55 single-amino acid $gp120_{JR-CSF}$ Ala mutants (*20*) and measured and analyzed their relative affinities for the gp120−CD4 complex (Table 2). The mutagenesis was directed by the structural information on the CD4i epitope recognized by 17b (*18*, *19*). The relative affinities were determined, as previously described (*21*), by comparing the half-maximal binding concentration for each mutant (complexed with CD4) to that for the wild-type $gp120_{JR-CSF}$ (complexed with CD4) (Table 2). For all mutants, we also investigated the binding of the CD4−IgG2 complex. Compared to the wild-type $gp120_{JR-CSF}$, single Ala substitution of eight residues (C119, K207, G367, M426, W427, V430, I423, and K432) resulted in a ≥ 3-fold reduction in the apparent binding affinity of Fab X5. The Ala substitution of residues C119 and K207 may affect the overall structure of gp120 because C119 is involved in the formation of a disulfide bridge (with residue C205) and K207 in a salt bridge (with residue E381), thus stabilizing the
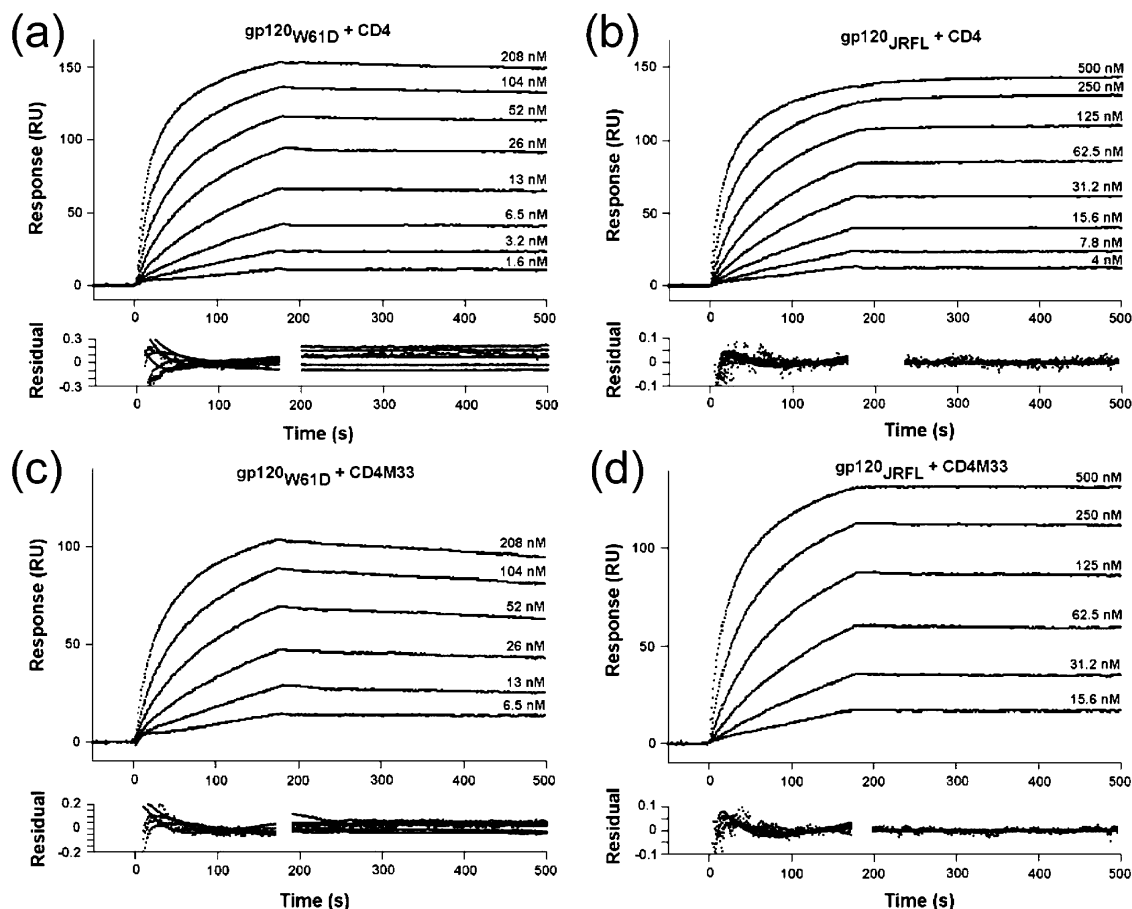
FIGURE 3: Specificity of X5 binding as determined by surface plasmon resonance (SPR). (a) Sensorgram overlays of gp120$_{W61D}$ (a and c) and gp120$_{JRFL}$ (b and d) in complex with CD4 (a and b) or CD4M33 mimic (c and d) binding to X5. Envelope proteins were preincubated with a 5-fold molar excess of CD4 or CD4M33 and injected at a rate of 30 μL/min at different concentrations (reported above the sensorgrams) over a B1 sensor chip, containing Fab X5 immobilized at 250 RU. The SPR response was recorded as a function of time, and kinetic rates were calculated by fitting both association and dissociation phases with a 1:1 Langmuir global model. The quality of the fitting was demonstrated by the relative residual plots (bottom panels) where the difference between the experimental and fitted data is distributed about the *X*-axis.
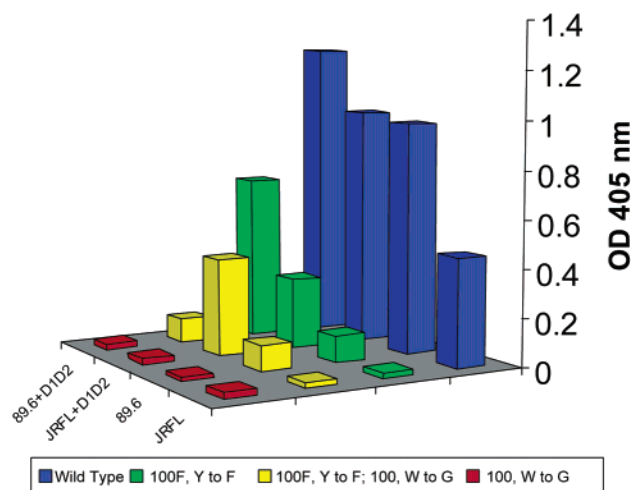

FIGURE 4: Site-directed mutants of Fab X5 and their gp120 binding activities in comparison with that of wild-type Fab.

relative orientation of the inner and outer domain of gp120 (*19, 22, 23*). Residues G367, M426, W427, and V430 may interact with CD4 (*19*) because mutations of these residues significantly affected CD4 binding (*21, 23*); the reduced level of CD4 binding could in turn account for the observed reduction in the level of X5 binding. The two remaining

substitutions, I423A and K432A, did not significantly affect CD4 binding and may therefore directly interact with X5.

Fine Mapping of the X5 Epitope. We suggest that the X5 epitope is in the proximity of the CD4 and coreceptor binding sites, as previously hypothesized on the basis of the results from competition studies of X5 and hMAbs with known specificities (*4*). The proposed location of the X5 epitope is in the vicinity of I423 and K432 (Figure 5a). For comparison, the functional footprints of CCR5 (*22*) and 17b (*23*), the 17b epitope, and the CD4 binding site (*18, 19*) are also depicted (Figure 5). In agreement with previously published results, the proposed X5 epitope overlaps that of 17b. The X5 epitope is likely very close to, but does not overlap with, the CCR5 footprint. The X5 epitope is also very close (closer than the 17b epitope) to the CD4 binding site, but does not overlap it (Figures 5).

To understand the basis for the cross-neutralizing activity of X5, we analyzed the extent of conservation of gp120 residues I423 and K432. Sequence alignment of 60 gp120 proteins from diverse HIV-1, HIV-2, and SIV isolates suggests that residues 417, 418, 420, 422, 423, 425, 427, 430−432 are highly conserved (>80% identical), residues 419, 421, 424, and 428 are partially conserved (>90% conservation of charge and hydrophobicity), and residues 426, 429, 433, and 434 are not conserved (Figure 6).

Table 2: Binding of X5 to Alanine Scanning Mutants of gp120$_{JR-CSF}$ Complexed with CD4[a]

gp120$_{JR-CSF}$[b]	gp120 domain[c]	relative affinity[d]	gp120$_{JR-CSF}$[b]	gp120 domain[c]	relative affinity[d]
wild type[e]		100	P417A	C4	153
C119A[f]		10	R419A[g]	C4	61
V120A		68	**I420A**[g]	C4	44
K121A[g]	C1 (V1/V2 stem)	77	K421A[g]	C4	66
L122A	C1 (V1/V2 stem)	43	**Q422A**[g]	C4	23
T123A[h]	C1 (V1/V2 stem)	60	**I423A**[g]	C4	2
L125A[h]	C1 (V1/V2 stem)	104	I424A	C4	78
V127A	C1 (V1/V2 stem)	116	N425A[h]	C4	105
T198A	C1 (V1/V2 stem)	98	**M426A**[h]	C4	25
S199A[h]	C1 (V1/V2 stem)	28	**W427A**[h]	C4	0
V200A[g]	C1 (V1/V2 stem)	81	Q428A[h]	C4	130
I201A	C1 (V1/V2 stem)	97	E429A[h]	C4	92
T202A	C1 (V1/V2 stem)	78	**V430A**[h]	C4	0
Q203A[g]	C2	93	G431A	C4	84
K207A[f]	C2	0	**K432A**[g]	C4	19
S256A[h]	C2	77	**M434A**[g]	C4	22
T257A[h]	C2	88	**Y435A**[g,h]	C4	26
R298A	C2	29	**P437A**[g]	C4	40
N339A	C3	77	R469A	V5	53
P363A	C3	76	P470A	V5	50
S365A[h]	C3	50	G471A	V5	62
G366A[h]	C3	38	**G472A**	C5	30
G367A[h]	C3	13	**G473A**[h]	C5	2
D368A[h]	C3	33	D474A[h]	C5	109
P369A[h]	C3	120	M475A	C5	62
E370A[h]	C3	46	R476A	C5	78
N386A	C3	60	D477A	C5	87
N392A	V4	36	W479A	C5	83

[a] Mutants with a more than 2-fold decrease in the level of X5 binding are highlighted in bold. [b] The residue numbering scheme is based on the sequence of prototypic HxBc2 gp120. [c] C is the constant domain and V the variable loop. [d] Calculated using the formula [apparent affinity (wild type)/apparent affinity (mutant)] × 100%, where apparent affinities were calculated as the antibody concentration at 50% maximal binding (*21*). [e] Wild-type JR-CSF gp120. [f] Residues involved in maintaining the overall structure of gp120. [g] Residues that exhibit decreased solvent accessibility in the presence of Fab 17b in the ternary complex. [h] Residues that exhibit decreased solvent accessibility in the presence of CD4 (D1D2) in the ternary complex.

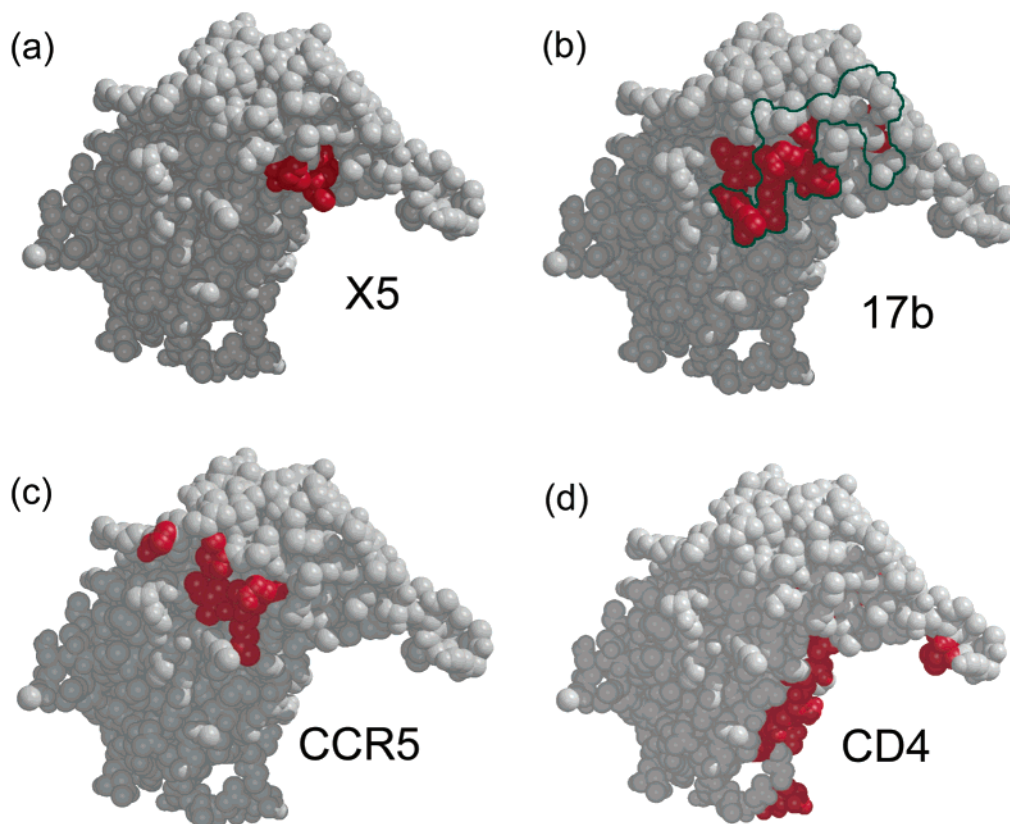

FIGURE 5: Comparison of the functional footprints on gp120 as defined by site-directed mutagenesis and crystallography: (a) X5 (this work), (b) 17b (*23*), (c) CCR5 (*22*), and (d) CD4 (PDB entry 1G9M). The green outline in panel b illustrates the contact area of 17b as seen in the crystal structure of the gp120−CD4−17b complex (*19*). This figure was generated using BOBSCRIPT (*24*) and RASTER3D (*25*).
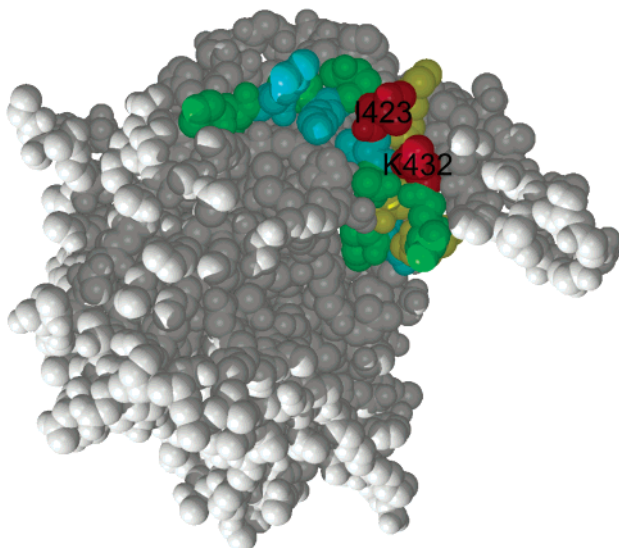
FIGURE 6: Space-filling model showing the conservation of gp120 residues in the X5 binding region (residues 417−434). Sequence alignment of 60 diverse primary immunodeficiency viruses was done using RPS-BLAST (CCD version 1.60, National Institutes of Health, Bethesda, MD). Residues colored red (423 and 432, in the proposed X5 epitope) or green (417, 418, 420, 422, 425, 427, 430, and 431) are highly conserved (>80% identical); those in cyan (419, 421, 424, and 428) are partially conserved (>90% conservation of charge and hydrophobicity), and those in yellow (426, 429, 433, and 434) are not conserved. This figure was generated using BOBSCRIPT (*24*) and RASTER3D (*25*).

Furthermore, these residues are located in a highly conserved area of residues (417−434), suggesting the possibility of a conserved three-dimensional framework. When the comparison was extended to 400 gp120 isolates, I423 was found in 387 and K432 and R432 were found in 295 sequences, suggesting that residue 432 is conserved in terms of the size and charge of the side chain.

The X5 epitope is a potential target for the development of HIV-1 entry inhibitors, and the protruding hook shape of CDR H3 may be useful for developing small molecule inhibitors. For some HIV-1 isolates, the neutralizing activity of IgG1 X5 is significantly lower than that of Fab X5 and scFv X5, partially because of spatial constraints at the virus−cell interface (*8*). Therefore, the use of the X5 epitope or its mimics as vaccine immunogens that elicit IgG1 X5 alone may not lead to effective HIV-neutralizing humoral responses. However, in combination with vaccine immunogens that can elicit antibodies that are able to induce the X5 epitope before the binding of HIV to CD4, the X5 epitope could be a component of effective vaccine immunogens. These observations and the fine mapping of the X5 epitope should be taken into account when designing HIV vaccine immunogens.

ACKNOWLEDGMENT

REFERENCES

1. Dimitrov, D. S. (2000) Cell biology of virus entry, *Cell 101*, 697−702.

2. Eckert, D. M., and Kim, P. S. (2001) Mechanisms of viral membrane fusion and its inhibition, *Annu. Rev. Biochem. 70*, 777−810.

3. Dimitrov, D. S. (1996) Fusin: a place for HIV-1 and T4 cells to meet, *Nat. Med. 2*, 640−641.

4. Moulard, M., Phogat, S. K., Shu, Y., Labrijn, A. F., Xiao, X., Binley, J. M., Zhang, M. Y., Sidorov, I. A., Broder, C. C., Robinson, J., Parren, P. W., Burton, D. R., and Dimitrov, D. S. (2002) Broadly cross-reactive HIV-1-neutralizing human monoclonal Fab selected for binding to gp120-CD4-CCR5 complexes, *Proc. Natl. Acad. Sci. U.S.A. 99*, 6913−6918.

5. Parren, P. W., and Burton, D. R. (2001) The antiviral activity of antibodies in vitro and in vivo, *Adv. Immunol. 77*, 195−262.

6. Burton, D. R., Pyati, J., Koduri, R., Sharp, S. J., Thornton, G. B., Parren, P. W., Sawyer, L. S., Hendry, R. M., Dunlop, N., Nara, P. L., et al. (1994) Efficient neutralization of primary isolates of HIV-1 by a recombinant human monoclonal antibody, *Science 266*, 1024−1027.

7. Saphire, E. O., Parren, P. W., Pantophlet, R., Zwick, M. B., Morris, G. M., Rudd, P. M., Dwek, R. A., Stanfield, R. L., Burton, D. R., and Wilson, I. A. (2001) Crystal structure of a neutralizing human IGG against HIV-1: a template for vaccine design, *Science 293*, 1155−1159.

8. Labrijn, A. F., Poignard, P., Raja, A., Zwick, M. B., Delgado, K., Franti, M., Binley, J., Vivona, V., Grundner, C., Huang, C. C., Venturi, M., Petropoulos, C. J., Wrin, T., Dimitrov, D. S., Robinson, J., Kwong, P. D., Wyatt, R. T., Sodroski, J., and Burton, D. R. (2003) Access of antibody molecules to the conserved coreceptor binding site on glycoprotein gp120 is sterically restricted on primary human immunodeficiency virus type 1, *J. Virol. 77*, 10557−10565.

9. Barbas, C. F., Burton, D. R., Scott, J. K., and Silverman, G. J. (2001) *Phage Display: A Laboratory Manual*, Cold Spring Harbor Laboratory Press, Plainview, NY.

10. Otwinowski, Z., and Minor, W. (1997) Processing of X-ray diffraction data collected in oscillation mode, *Methods Enzymol. 276*, 307−326.

11. Navaza, J. (1994) An automated package for molecular replacement, *Acta Crystallogr. A50*, 157−163.

12. Brünger, A. T., Adams, P. D., Clore, G. M., DeLano, W. L., Gros, P., Grosse-Kunstleve, R. W., Jiang, J. S., Kuszewski, J., Nilges, M., Pannu, N. S., Read, R. J., Rice, L. M., Simonson, T., and Warren, G. L. (1998) Crystallography & NMR system: A new software suite for macromolecular structure determination, *Acta Crystallogr. D54*, 905−921.

13. Collaborative Computational Project Number 4 (1994) The CCP4 Suite: Programs for Protein Crystallography, *Acta Crystallogr. D50*, 760−763.

14. Romesberg, F. E., Santarsiero, B. D., Spiller, B., Yin, J., Barnes, D., Schultz, P. G., and Stevens, R. C. (1998) Structural and kinetic evidence for strain in biological catalysis, *Biochemistry 37*, 14404−14409.

15. Jones, T. A., and Kjeldgaard, M. (1997) Electron-density map interpretation, *Methods Enzymol. 277*, 173−208.

16. Brünger, A. T., and Rice, L. M. (1997) Crystallographic refinement by simulated annealing: methods and applications, *Methods Enzymol. 277*, 243−269.

17. Martin, L., Stricher, F., Misse, D., Sironi, F., Pugniere, M., Barthe, P., Prado-Gotor, R., Freulon, I., Magne, X., Roumestand, C., Menez, A., Lusso, P., Veas, F., and Vita, C. (2003) Rational design of a CD4 mimic that inhibits HIV-1 entry and exposes cryptic neutralization epitopes, *Nat. Biotechnol. 21*, 71−76.

18. Kwong, P. D., Wyatt, R., Robinson, J., Sweet, R. W., Sodroski, J., and Hendrickson, W. A. (1998) Structure of an HIV gp120 envelope glycoprotein in complex with the CD4 receptor and a neutralizing human antibody, *Nature 393*, 648−659.

19. Kwong, P. D., Wyatt, R., Majeed, S., Robinson, J., Sweet, R. W., Sodroski, J., and Hendrickson, W. A. (2000) Structures of HIV-1 gp120 envelope glycoproteins from laboratory-adapted and primary isolates, *Structure 8*, 1329−1339.

20. Scanlan, C. N., Pantophlet, R., Wormald, M. R., Saphire, E. O., Stanfield, R., Wilson, I. A., Katinger, H., Dwek, R. A., Rudd, P. M., and Burton, D. R. (2002) The broadly neutralizing anti-human immunodeficiency virus type 1 antibody 2G12 recognizes a cluster of α1→2 mannose residues on the outer face of gp120, *J. Virol. 76*, 7306−7321.

21. Pantophlet, R., Ollmann Saphire, E., Poignard, P., Parren, P. W., Wilson, I. A., and Burton, D. R. (2003) Fine mapping of the interaction of neutralizing and nonneutralizing monoclonal antibodies with the CD4 binding site of human immunodeficiency virus type 1 gp120, *J. Virol. 77*, 642−658.

22. Rizzuto, C., and Sodroski, J. (2000) Fine definition of a conserved CCR5-binding region on the human immunodeficiency virus type 1 glycoprotein 120, *AIDS Res. Hum. Retroviruses 16*, 741−749.

23. Rizzuto, C. D., Wyatt, R., Hernandez-Ramos, N., Sun, Y., Kwong, P. D., Hendrickson, W. A., and Sodroski, J. (1998) A conserved HIV gp120 glycoprotein structure involved in chemokine receptor binding, *Science 280*, 1949−1953.

24. Esnouf, R. M. (1997) An extensively modified version of MolScript that includes greatly enhanced coloring capabilities, *J. Mol. Graphics Modell. 15*, 132−134.

25. Merritt, E. A., and Bacon, D. J. (1997) Raster3D: photorealistic molecular graphics, *Methods Enzymol. 277*, 505−524.

26. Nicholls, A., Sharp, K. A., and Honig, B. (1991) Protein folding and association: insights from the interfacial and thermodynamic properties of hydrocarbons, *Proteins: Struct., Funct., Genet. 11*, 281−296.